Piezoelectric Energy Harvesting System

for Low-Power IoT Sensors

Ivo Sokal
Vincent Verkoren

Subgroup 1: Piezoelectric Transducer Design and Characterization

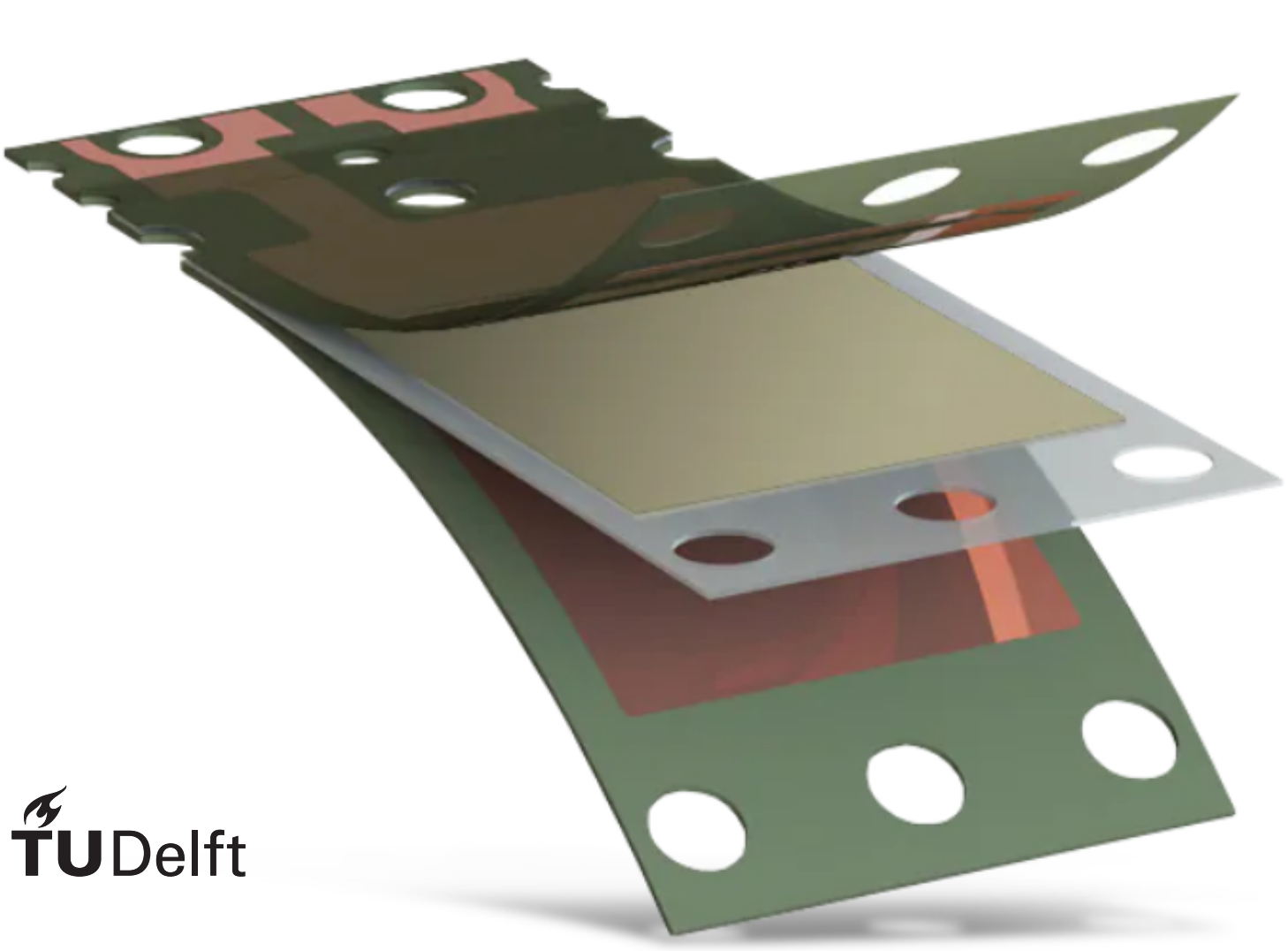

TU Delft

Piezoelectric Energy Harvesting System

for Low-Power IoT Sensors

by

Ivo Sokal
Vincent Verkoren

to obtain the degree of Bachelor of Science
at the Delft University of Technology,
to be defended publicly on Friday June 26, 2025 at 3:30 PM.

Student number:	Ivo Sokal	5506166
	Vincent Verkoren	5293847
Supervisor:	Dr. Sijun Du	TU Delft
Daily supervisors:	Wenyu Peng & Zijun Qui	TU Delft
Project duration:	April 21, 2025 – June 27, 2025	

TU Delft

Abstract

As the Internet of Things (IoT) continues to expand across various industries, the demand for self-generating and sustainable power solutions is increasing more urgent. Piezoelectric energy harvesters offer a promising solution as they can generate electrical energy from ambient mechanical vibrations and operate independently even in locations that are difficult to reach. This thesis explores the modeling and measurements of a piezoelectric harvesting (PEH) system designed to power a low-power IoT circuit embedded in aircraft wings. Focusing on a piezoelectric cantilever beam implementation made from a PZT-5H transducer, the research evaluates three commercial models developed by 'Mide Technology': PPA-1021, PPA-2011 and PPA-4011. Every model is evaluated for their performance under mechanical vibrations in the 30-120 Hz range, characteristic for aircraft environments. The methodology includes electromechanical modeling and a structured series of laboratory experiments to validate key parameters such as resonance frequency tuning, impedance matching, power output, and behavior in noisy environments. Among the tested models, the PPA-2011 demonstrated the best overall performance achieving a peak power output of 1.61 mW at resonance of 58 Hz and was able to stably power an IoT circuit even in a noisy environment. The results validate the ability to use PEHs for the power generation of aircraft wireless sensor networks. Future work should explore long-term stability and extensive testing of real-world aircraft vibrations.

Preface

The Bachelor Graduation Project has been an interesting and valuable ten-week exploration into the field of piezoelectric energy harvesting. Our work focused on modeling and characterizing commercial piezoelectric transducers to determine their suitability for powering low-power IoT sensors embedded in aircraft structures.

We express our gratitude to our supervisors, Dr. Sijun Du, Wenyu Peng, and Zijun Qui, for their continuous support and constructive feedback throughout the project. Their guidance was very helpful for the refinement of our research. We would also like to thank our fellow group members Remon van Bemmel, Laurens-Jan Cammeraat, Wester Landman and Alessio Solter, whose collaboration and shared resources enabled the successful integration of our work into a functioning prototype.

Ivo Sokal
Vincent Verkoren
Delft, June 2025

Contents

1 Introduction 1
1.1 Harvester . . . 1
1.2 Project objective . . . 1
1.3 Thesis outline . . . 1

2 Programme of requirements 3
2.1 Mandatory requirements . . . 3
2.1.1 Functional requirements . . . 3
2.1.2 Non-functional requirements . . . 3
2.2 Trade-off requirements . . . 4

3 Fundamentals of Piezoelectric Energy 5
3.1 Introduction . . . 5
3.2 How does it work? . . . 5
3.3 Models . . . 6
3.4 Harvester . . . 6

4 Modeling of the Piezoelectric Harvester 8
4.1 Mechanical part . . . 8
4.2 Electrical part . . . 9
4.3 Analysis and simulations . . . 9

5 Measurements and Experiments 11
5.1 Measurement procedure . . . 11
5.1.1 Step 1: Measure internal capacitance . . . 12
5.1.2 Step 2: Identify resonance frequency . . . 12
5.1.3 Step 3: Determine optimal load resistance and power output . . . 12
5.2 Experimental results . . . 12
5.2.1 Internal capacitance . . . 12
5.2.2 Resonance frequency and power output . . . 12
5.3 Measurements with noise . . . 14

6 Prototype implementation 16

7 Discussion 17
7.1 Effect of tip mass on resonance frequency and power output . . . 17
7.2 Performance across PET models . . . 17
7.3 Impact of noise on energy harvesting . . . 17

8 Conclusion 19

9 Future work 20
9.1 Real-world vibration testing . . . 20
9.2 Extract complete electromechanical modeling . . . 20
9.3 Create a physics model . . . 20
9.4 Thermal performance . . . 20
9.5 Regulatory and environmental testing . . . 21
9.6 Self-tuning harvester systems . . . 21

Appendices 24

A Appendix 25
A.1 Frequency Response Simulations . . . 25
A.2 Python code for noisy conditions . . . 26

1 Introduction

With the ongoing expansion of the Internet of Things (IoT), the need for sustainable and maintenance-free power sources is becoming increasingly important. Currently, many IoT sensors are powered by non-rechargeable batteries, which require frequent replacement, or through direct wiring, which adds weight, complexity, and cost. This challenge is especially prominent in the aerospace industry. Modern aircraft have a dense network of sensors embedded throughout their structure to monitor many different types of environmental and structural data. As these sensors often reside in difficult to access areas, such as within the wings or fuselage, it makes battery replacement or wiring costly and impractical. Piezoelectric energy harvesters (PEHs) offer a promising alternative [21], as they can generate electrical energy from ambient mechanical vibrations and operate independently even in hard-to-reach locations [23].

1.1. Harvester

The piezoelectric harvester used in this project is based on a cantilever beam. This harvester consists of a piezoelectric transducer (PET) fixed at one end and loose at the other. By adding weight to the free end, the resonance frequency of the cantilever can be adjusted. Mechanical vibrations induce strain within the piezoelectric layers of the transducer, which in turn generates power. By tuning the resonance frequency of the cantilever to match typical aircraft vibration frequencies, the harvester can achieve maximum power transfer.

1.2. Project objective

The objective of this project is to design, model and experimentally validate a piezoelectric energy harvesting (PEH) system suitable for use in aircraft environments. The focus of Subgroup 1, detailed in this thesis, is on the selection, modeling and characterization of commercial piezoelectric transducers (PETs) that can operate effectively within the typical vibrational frequency band encountered in aircraft structures.

This includes identifying an optimal PET model, tuning its resonance frequency for maximum power output, measuring key electrical characteristics such as internal capacitance and impedance, and evaluating its performance under both controlled and noisy vibration scenarios.

The work of Subgroup 1 forms the foundation for the broader system. Subgroup 2 builds upon our results by designing a power conditioning circuit to rectify and regulate the harvested energy. Subgroup 3 integrates the complete system with a low-power IoT sensor. Together, these efforts aim to demonstrate a fully functional, maintenance-free power supply for aircraft-embedded IoT sensors.

1.3. Thesis outline

The outline of this thesis is as follows. In Chapter 2 the requirements of the project are discussed. After that, in Chapter 3 the fundamentals and history of piezoelectric technology are described. The chapter takes a deep dive into the operation of piezoelectric materials, including direct and converse piezoelectric effects,

common material types, and their applications in energy harvesting systems. The chapter is followed by Chapter 4, which gives an overview on how to model and simulate such PEHs. In Chapter 5 the measurement setup is shown, followed by the measurement procedure, and most importantly the measurement results are highlighted. The chapter describes decisions that are made on how to measure ideal but also real-world scenarios on the different available PET models. Chapter 6 outlines the system integration with the other subgroups. Whereas Chapter 7 discusses the simulations and measurements that are made. The purpose of this chapter is to evaluate the key findings and evaluate the performance of the different PET models. In Chapter 8 the conclusions for this project are drawn, and in Chapter 9 finally our recommendations for potential future work are given.

2

Programme of requirements

The goal of subgroup 1 is to characterize, and evaluate different piezoelectric transducer (PET) models for a piezoelectric energy harvester (PEH) capable of powering low-power IoT sensors within an aircraft wing. The PET should operate reliably under real aircraft vibration conditions (10–300 Hz [1]) and generate sufficient power for sensor operation for professional aerospace applications.

The PoR includes both functional and non-functional key requirement indicators, along with conditions related to its behavior, performance and working. The version of the PoR presented in the following sections will be used to assess the different PET models and conclude which model would fit the overall IoT system the best.

2.1. Mandatory requirements

These criteria represent the minimum standards the piezoelectric energy harvester (PEH) must meet. They are divided into functional and non-functional requirements: functional requirements specify what the system must do, while non-functional requirements define the attributes the system must possess.

2.1.1. Functional requirements

1. The resonance frequency of the PEH must be between 30-120 Hz to operate optimally within an aircraft environment
2. The system must operate passively without any external power input
3. The PEH must be capable of impedance-matched output to maximize power delivery to the IoT circuit
4. The PEH must generate at least 6.2 V peak to peak at resonance
5. The PEH must deliver on average 250 μW
6. The PEH must maintain continuous operation during typical aircraft flight durations (up to 10 hours) without performance degradation

2.1.2. Non-functional requirements

1. PEH should charge the required capacitor even when white noise in the range of 10-300 hz with amplitude of 0.6 times the produced signal wave is present
2. The PEH should be easy to tune to different resonance frequencies by adjusting the tip-mass
3. The tip of the PET shall not vibrate at an offset larger than 2 cm
4. The PEH must operate within the aircraft cabin and fuselage temperature range of -40°C to +85°C.

2.2. Trade-off requirements

These are criteria of which it is preferable to comply with as much as possible.

1. Select the transducer model to balance cost, complexity, and power output.
2. The PEH system should be simple to connect and integrate into the IoT circuit
3. The PEH should operate under EUROCAE ED-14G tests

3

Fundamentals of Piezoelectric Energy

3.1. Introduction

The piezoelectric effect was first demonstrated in the 1880s by two brothers, Pierre and Jacques Curie [16]. They showed that certain crystals, when subjected to mechanical deformation, create a voltage. However, the brothers did not discover that the inverse is also true. Applying a voltage to the crystal would induce stress in the crystal. This effect was discovered some years later by Lippmann. The first real applications of the piezoelectric effect took place in World War I. During this time it was used in sonar devices for submarines [4].

After this time, development continued but was limited by the quality of material available at that time. However, when World War II took place, research intensified and in 1952 the Tokyo Institute of Technology created a new ceramic piezoelectric type material, lead zirconium titanate (PZT). Compared to other crystal types, PZT ceramic shows greater sensitivity, higher operating temperatures and more strength [22]. These advances also lead to a new way to develop piezoelectric devices for specific applications.

Later in the 20th century the commercial market for piezoelectric materials has grown and more advanced piezo products are being made. Today, piezoelectric materials are used in many industrial, medical and consumer applications. However, in the last decades more interest is growing in the way that piezoelectricity can generate sustainable energy. Piezoelectric elements are an excellent application for this since they are able to generate power from mechanical vibrations without the need for an external power source [20].

3.2. How does it work?

The term "piezoelectricity" refers to the relationship between pressure and electricity that exists within a certain material [8]. When mechanical stress is applied to a piezoelectric material, such as pressure or deformation, it changes the position of atoms in the piezoelectric material. These changes cause the positive and negative charges in the unit cell of the crystal to separate, as can be seen in Figure 3.1. As a result, an electric dipole is created within each crystal unit, where one side of the crystal becomes positively charged and the other side becomes negatively charged. Due to this, a voltage is induced over the whole crystal. When the mechanical stress is removed, the material returns to its original, stable state.

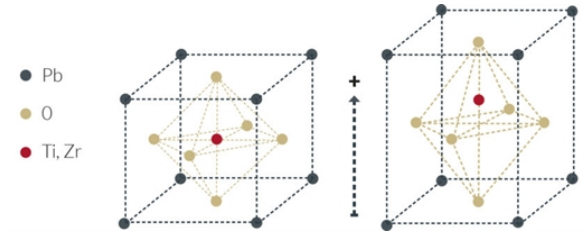

Figure 3.1: PZT crystal structure
Source: [17]

Piezoelectric elements can be crystals or specially made ceramics. In this project, all piezoelectric transducers are made using piezoelectric ceramic PZT. This material is made from a combination of lead zirconate (PbZrO3) and lead titanate (PBTiO3). These ceramics are made up of crystal-like structures, called crystallites, that are initially oriented randomly within the ceramic [11]. As a result, the overall polarization of the material is zero, meaning the ceramic does not show piezoelectric properties.

To activate the effect, after producing the ceramic, the material has to be poled. At a certain temperature, a DC electric field is applied and the crystallites are aligned. This process can be seen in Figure 3.2. After the electric field, also called the poling field, is removed, the ceramic retains its polarization and has piezoelectric properties. Now when the material is exposed to stress, a voltage is induced.

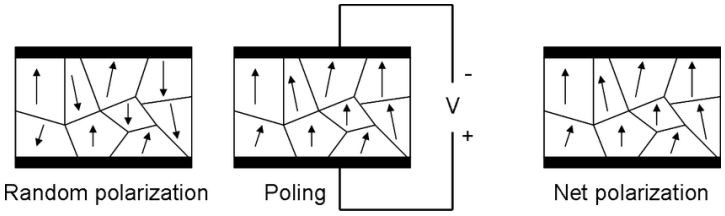

Figure 3.2: Poling process
Source: [10]

Within the lead zirconate titanate (PZT) family of piezoelectric materials there are different types [6]. For example: PZT-4, PZT-5A, PZT-5H. The main differences between the types are their behavior with respect to the temperature and stiffness of the ceramic. In this project, all harvesters use PZT-5H. The latter offers the best piezoelectric properties but is more sensitive to temperature changes.

3.3. Models

For this project, ready-made piezoelectric harvesters are used from the brand "Mide" [3]. The used models are the PPA-1021, PPA-2011 and PPA-4011 [3]. As mentioned, all these models use PZT-5H as the piezoelectric material.

The main differences between the models are their dimensions. Additionally, the PPA-1021 has one PZT layer, PPA-2011 has two PZT layers and the PPA-4011 four layers. Every model has the same layering principle: Each layer of PZT-5H has a layer of copper above and below, which acts as conducting layers for the PZT-5H layers. Each of these three layers is separated by FR4 epoxy. This is a glass-reinforced epoxy laminate material that is often found in printed circuit boards (PCBs). Since these FR4 layers are so thin, they can be ignored for analysis. See the manufacturer's datasheet [3] for all available specifications.

3.4. Harvester

There are multiple ways to use PZT elements to harvest energy. However, the most widely used harvester structure is the piezoelectric cantilever beam. Since it can generate the most power from mechanical vibra-

tions. In this setup the PZT plate is fixed on one end and free on the other end. This results in the PZT plate to act as a bimorph cantilever beam as can be seen in Figure 3.3.

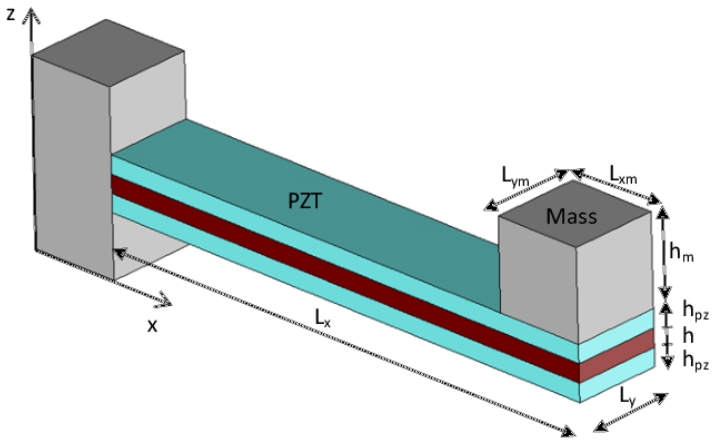

Figure 3.3: Piezoelectric cantilever beam
Source: [7]

Vibrating the harvester will cause the tip of the PET to displace, which will produce strain on the layers. This results in an alternating voltage being generated through the electrodes. By adjusting the tip mass, the resonant frequency and displacement of the cantilever beam can be adjusted.

4

Modeling of the Piezoelectric Harvester

To better understand and predict the behavior of the PEH, a comprehensive electromechanical model is developed. This model incorporates the mechanical dynamics of the vibrating beam, the electrical response of the piezoelectric material, and the coupling mechanism that reflects the energy conversion between the two domains. All parts of the PEH can be modeled using circuit elements, as demonstrated in [19]. This model can be created using the electro-mechanical analogy. Using the equivalence between the differential equations applied in the mechanical and electrical world, an electromechanical coupling can be made. The equivalent circuit for this model can be seen in Figure 4.1.

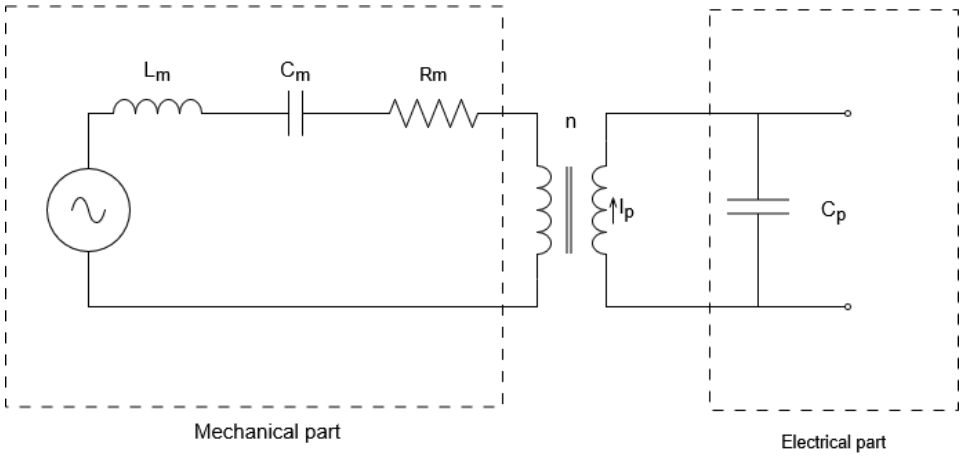

Figure 4.1: Equivalent circuit of the PEH

In the mechanical part currents are equivalent to the mass oscillation velocities and voltages are equivalent to the forces acting on the PEH [18]. The transformer in the middle represents the piezoelectric coupling, which transforms mechanical energy into electrical voltage. This model is based on the Butterworth-van-Dyke circuit, which is often used to model the electrical behavior of resonators [13].

4.1. Mechanical part

The mechanical part of the model can be seen as a second-order mass-spring-damper system [2]. This corresponds to Newton's second law for a damped harmonic oscillator.

$$F(t) = m\frac{d^2x}{dt^2} + c\frac{dx}{dt} + kx(t) \tag{4.1}$$

This time-domain differential equation can be described as an RLC circuit.

$$v(t) = L\frac{di(t)}{dt} + Ri(t) + \frac{1}{C}\int i(t)\,dt \tag{4.2}$$

$$\frac{dv(t)}{dt} = L\frac{d^2i(t)}{dt^2} + R\frac{di(t)}{dt} + \frac{1}{C}i(t) \tag{4.3}$$

Applying the electromechanical coupling, equating 4.1 with 4.3 results in the following coupling:

- The inductance L_m: Represents the effective mass, including the tip mass contribution
- The capacitance $C_m = 1/k_{eff}$, corresponds to the inverse of the effective stiffness k_{eff}
- The resistance R_m, models the mechanical losses

4.2. Electrical part

The electrical part can be modeled as the internal capacitance C_p of the PET. Using this model, the mechanical side of the circuit is treated as an uncoupled mechanical system. The perfect transformer, with a coupling factor N, can be seen as the piezoelectric coupling from mechanical to electrical domain. The coupling factor is directly proportional to the charge constant d_{31} of the piezoelectric material. This constant is a property of the material and describes how well a force is converted into charge [15]. The subscript d_{ik} tells us in which direction i of the PET the electric charge appears while we apply a force in direction k. The constant is expressed in Coulomb/Newton.

When the PEH vibrates at or near resonance, the impedances of the inductor L_m and C_m cancel out, leaving only the mechanical resistance left. This means that the system is only limited by mechanical damping, leading to maximum mechanical vibration or displacement. In this case, to simplify calculations, the model can be seen as a current source in parallel with the internal capacitance C_p and internal resistance R_p [5], as shown in Figure 4.2.

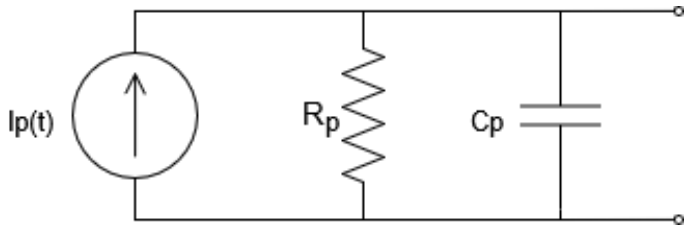

Figure 4.2: Equivalent circuit of the PEH at or near resonance

The current source I_p is directly related to the variation in strain within the PET produced by the applied force. When the PET is excited at its resonant frequency by a sinusoidal vibration, I_p can be modeled as a sinusoidal current source.

$$I_p(t) = I_0 sin(\omega_0 t) = I_0 sin(2\pi f_0 t) \tag{4.4}$$

Here, I_0 is a function of the excitation amplitude (or acceleration) and f_0 is the resonance frequency.

4.3. Analysis and simulations

With the equivalent circuit model established, simulations were conducted to analyze the mechanical behavior of the PET under harmonic excitation. The aim of these simulations was not to predict voltage or current output, but rather to confirm the resonance characteristics of each device under different tip mass conditions. All simulations were implemented in LTSpice using the extracted or derived parameters from the datasheet

[3] and measured values. In this section the simulation of the PPA-2011 is shown. The rest of the simulations can be found in Appendix A.1. Figure 4.3 shows the simulated frequency response of the PPA-2011. In Table 4.1 the values for the resonance peaks are summarized.

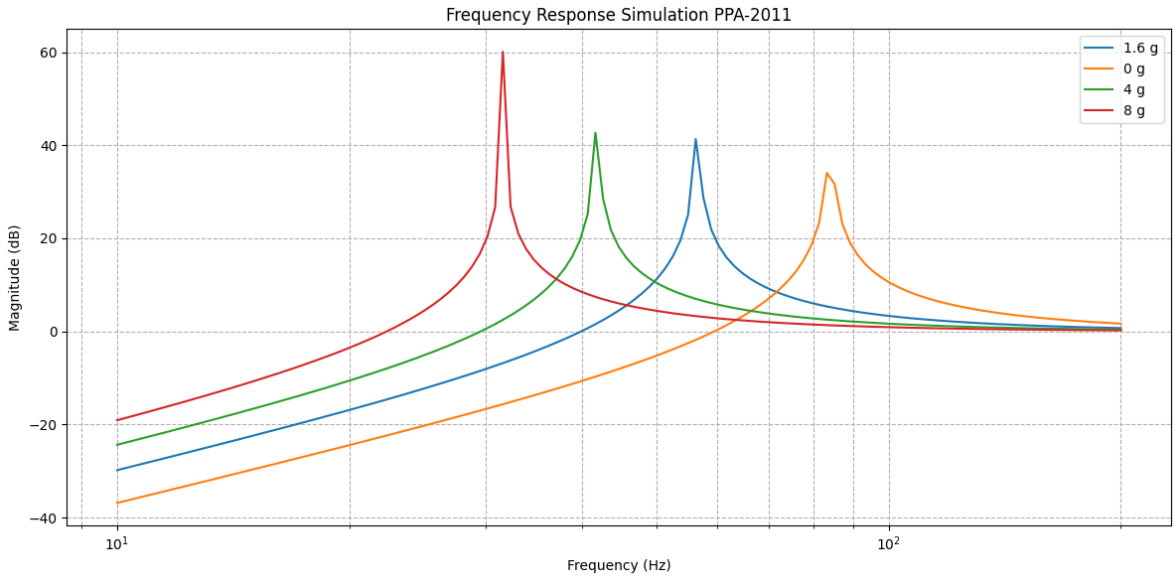

Figure 4.3: Frequency Response simulation PPA-2011 with different tip mass configurations

Table 4.1: Resonance peaks of simulation for different tip masses

Tip Mass (g)	f_r **(Hz)**
0	84
1.6	56
4	41
8	32

It is important to note that the simulations presented here only consider the mechanical branch of the equivalent circuit. The piezoelectric coupling and the electrical domain that is modeled as a current source in parallel with the internal capacitance C_p were not included in the simulations.

However, the electrical part of the equivalent circuit, including the sinusoidal current source described in Equation 4.4, was used by other subgroups within the project to simulate power conditioning and energy storage circuits. By providing the measurements to the other subgroups, an ideal sinusoidal current source operating at the resonance frequency, in parallel with C_p, could be simulated to evaluate rectifier efficiency and load behavior.

Further integration of the electrical and mechanical branches would require a more detailed model of the coupling coefficient, which was not extracted in this work.

5

Measurements and Experiments

In order to validate the simulation models and characterize the performance of the selected PETs under real-world conditions, a series of experiments were conducted. These experiments aimed to identify key electrical and mechanical parameters of the transducers, such as resonance frequency, internal impedance, and power output under various loading and excitation conditions. This chapter provides an overview of the measurement methodology, experimental setup, and results.

To systematically extract the optimal configuration for each transducer, the following steps were taken: measuring internal capacitance, sweeping through frequencies to identify resonance, tuning the tip masses for frequency alignment, and finally, performing power output measurements under both clean and noisy excitation conditions.

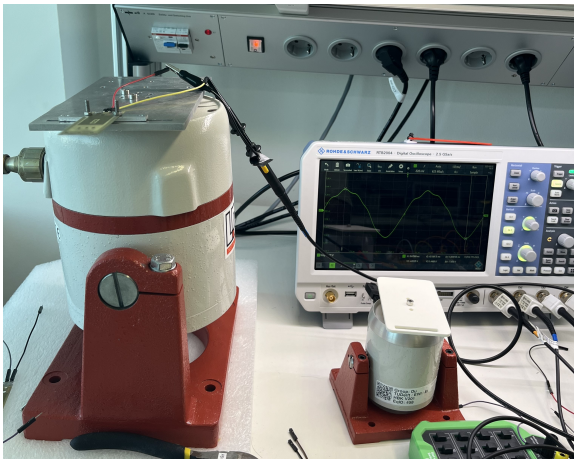

Figure 5.1: Measurement setup including both shaker models

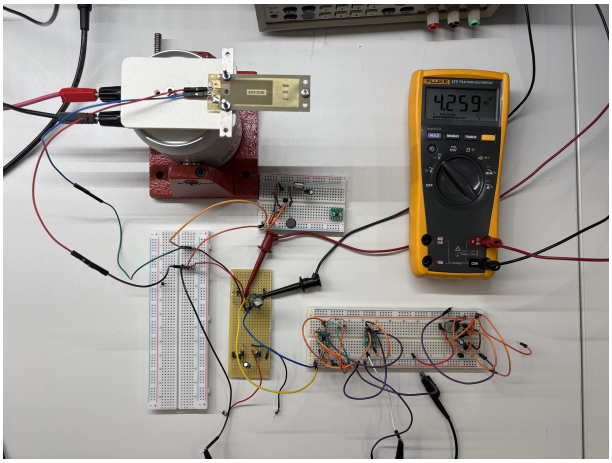

Figure 5.2: Measurement setup including power conditioning circuit

Figures 5.1 and 5.2 show the shaker setup that is used for the measurements. This includes two different shakers, a small and a bigger model. Specifically, LDS V201 and LDS V406 [9]. It contains a PET mounting plate and the PET that is mounted using two bolts and nuts. The shaker is driven by a Tektronix AFG 3021B function generator, where for the LDS V406 shaker, a complementary voltage amplifier is necessary. The output of the PET is then measured using a Tektronix TBS 2000 Series digital oscilloscope.

5.1. Measurement procedure

To characterize and compare the performance of the available PET models, a structured measurement procedure was implemented. The transducers tested were the following: PPA-1021, PPA-2011, and PPA-4011 [3]. These different models differ in dimensions, capacitance, and mechanical response. All measurement steps

were repeated across these models to ensure consistency. In this way a comparison can be made to see which model fits best with the specific needs in this project.

5.1.1. Step 1: Measure internal capacitance

The internal capacitance C_p of each PET was measured using a standard LCR meter. Although nominal capacitance values are provided in the manufacturer's datasheet, small deviations are expected as a result of manufacturing tolerances. C_p influences the electrical behavior and simulation accuracy. Therefore, it was necessary to implement this in the measurement procedure.

5.1.2. Step 2: Identify resonance frequency

To determine the resonance frequency f_r of each PET, a frequency sweep was performed using the shaker setup. A sinusoidal signal was generated to drive the shaker and different voltage amplitudes were measured across the PET on the oscilloscope. In theory, the voltage peak should be highest when the PET vibrates at its resonance frequency. In this way, the optimal frequency of every PET can be found.

To adjust the resonance frequency, weights can be added to the free end of the vibrating PET beam. The more weight attached, the lower the resonance frequency becomes. In this way, the resonance frequency of the PET can be tuned. Tip masses ranging from 0 to 18 grams were incrementally mounted to shift the resonance frequency.

5.1.3. Step 3: Determine optimal load resistance and power output

The power output of the different PET models is analyzed. By connecting a variable resistor box across the PET output, the voltage across the load was measured for different resistance values. The power output is calculated using the formula:

$$P = \frac{V_{rms}^2}{R}.$$

The goal is to match the resistance of the box with the internal resistance of the PET. This matched resistance condition is expected to yield optimal power transfer due to impedance matching between the PET and the load.

5.2. Experimental results

5.2.1. Internal capacitance

Table 5.1 summarizes the measured internal capacitance of each transducer model. The results show slight deviations from the values reported in the datasheet [3], highlighting the importance of empirical validation for accurate modeling and simulation.

Table 5.1: Measured internal capacitance of piezoelectric transducer models

Model	**PPA-1021**	**PPA-2011**	**PPA-4011**
C_p (nF)	22.8	189.3	436

5.2.2. Resonance frequency and power output

A frequency sweep was performed for each PET using different tip masses. The goal was to observe the shift in resonance frequency and the corresponding output power. Figures 5.3-5.8 show the measured frequency response and power output curves, while Tables 5.2-5.4 present the corresponding numerical results.

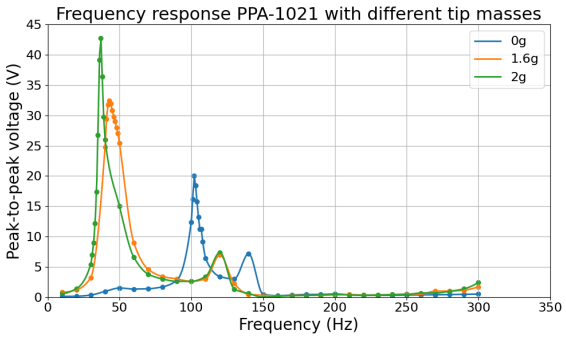

Figure 5.3: Frequency response of PPA-1021

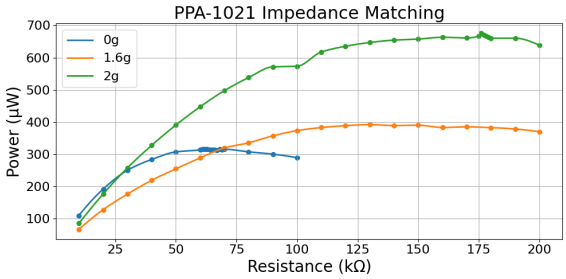

Figure 5.4: Power output of PPA-1021

Table 5.2: Performance of PPA-1021 under varying tip mass

Tip Mass (g)	f_r **(Hz)**	R_i **(kΩ)**	**Power** (μ**W)**
0	102	63	316
1.6	43	131	392
2	37	179	664

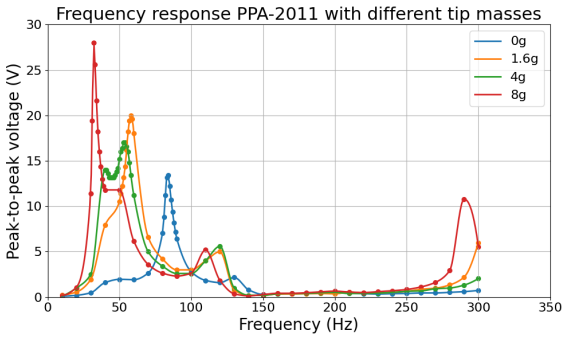

Figure 5.5: Frequency response of PPA-2011

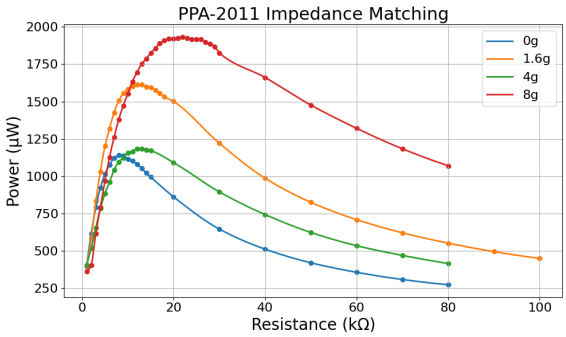

Figure 5.6: Power output of PPA-2011

Table 5.3: Performance of PPA-2011 under varying tip mass

Tip Mass (g)	f_r **(Hz)**	R_i **(kΩ)**	**Power (mW)**
0	84	9	1.14
1.6	58	12.5	1.61
4	54	13.5	1.18
8	32	21.5	1.93

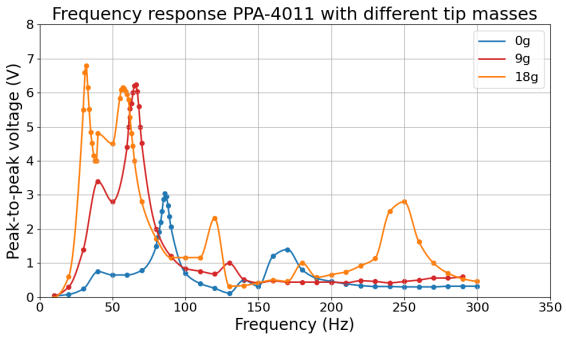

Figure 5.7: Frequency response of PPA-4011

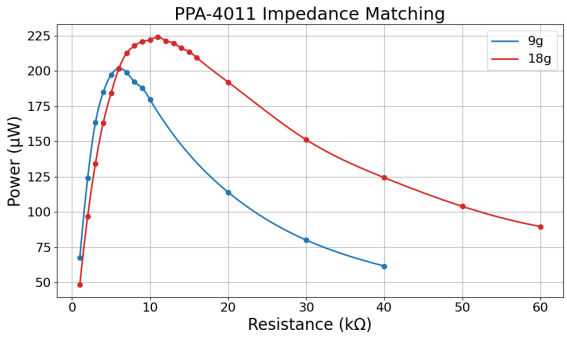

Figure 5.8: Power output of PPA-4011

Table 5.4: Performance of PPA-4011 under varying tip mass

Tip Mass (g)	f_r **(Hz)**	R_i **(kΩ)**	**Power** (μ**W)**
0	86	4.5	23
9	66	5.5	201
18	32	10	222

What is clearly noticeable is that the resonance frequency peaks decrease as the tip mass increases. This is in line with expectations as increasing the tip mass on a vibrating cantilever will increase the inertia without increasing stiffness. Peak power output varies by model and configuration, with PPA-2011 showing the most promising performance. A more detailed interpretation is provided in Chapter 7.

5.3. Measurements with noise

Earlier measurements were conducted using a near-perfect sinusoidal signal generated by a signal generator. Although useful for benchmarking and initial characterization, these conditions are not representative of real-world applications. In practice, such as on the surface of an aircraft wing during flight, vibrations are rarely clean or periodic. Instead, they consist of a complex superposition of multiple frequency components. This can significantly affect the performance of PEHs and should be considered in the characterization process.

To evaluate how the PET behaves under more realistic conditions, custom waveforms were constructed that simulate ambient mechanical vibrations. These waveforms were generated in Python and consist of 43 Hz, 58 Hz and 66 Hz sine waves, representing a dominant frequency component, combined with bandpass-filtered white noise. The choice of frequencies is made because these values were closest to the target frequency of 60 Hz. This target is chosen because the PPA-2011 model giving the highest output at 32 Hz does not align with non-functional requirement one. A part of the frequency peak was outside the 30-120 Hz frequency band, as can be seen in Figure 5.6. The second highest power output is given by the same model at 58 Hz. The values have been derived from Tables 5.2, 5.3 and 5.4. The noise was filtered in the frequency range of 10–300 Hz [1], which approximates the typical spectrum of structural vibrations encountered in aircraft applications. The noise was scaled by the amplitude to approximately 20%, 60% and 80% of the sine wave component and then added to the sine wave. The resulting signal was normalized to fit within the ±1 range, ensuring compatibility with simulation and signal generation hardware. The Python code can be found in the Appendix A.2. The noise waveforms are shown in Figures 5.9, 5.11 and 5.13 below.

This noise waveform was used to drive the shaker. By doing this, it could be examined how noise and off-resonance components impact the harvested power compared to idealized single-frequency excitation. In addition, it allows us to assess the robustness of the harvester under realistic operating conditions.

The power output of the PETs under these noisy input conditions is shown in Figures 5.10, 5.12 and 5.14 and compared to earlier results obtained under clean sinusoidal excitation.

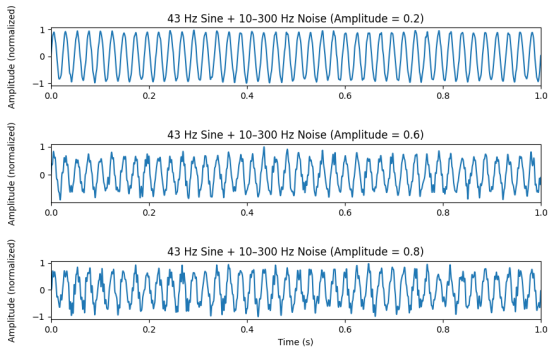

Figure 5.9: 43 Hz sine wave combined with 10–300 Hz noise at varying amplitudes.

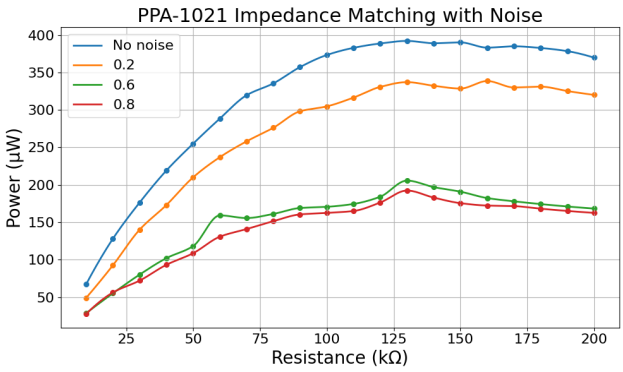

Figure 5.10: Power output PPA-1021 with a 1.6 gram tip mass under noisy input conditions

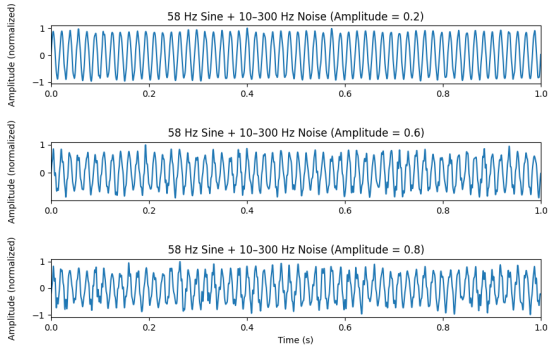

Figure 5.11: 58 Hz sine wave combined with 10–300 Hz noise at varying amplitudes.

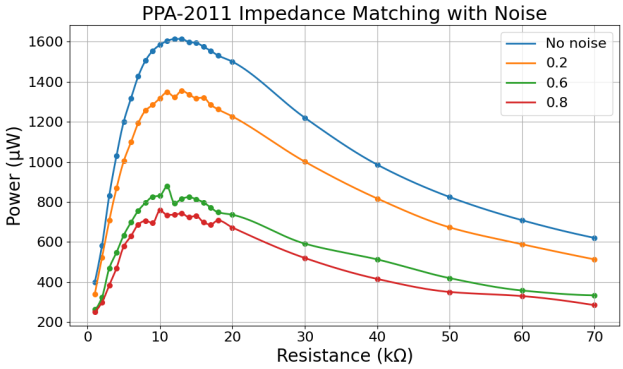

Figure 5.12: Power output PPA-2011 with a 1.6 gram tip mass under noisy input conditions

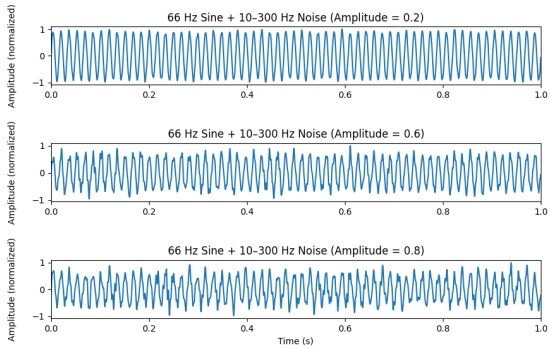

Figure 5.13: 66 Hz sine wave combined with 10–300 Hz noise at varying amplitudes.

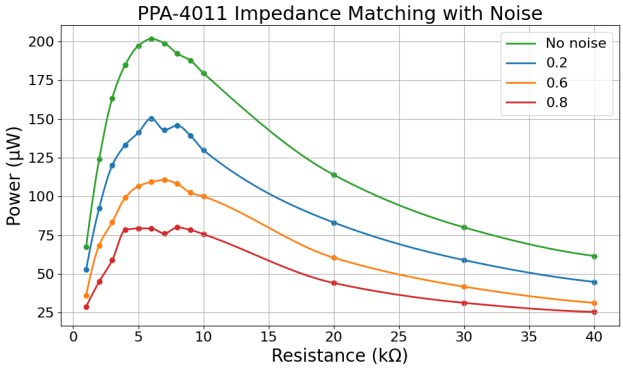

Figure 5.14: Power output PPA-4011 with a 9 grams tip mass under noisy input conditions

6

Prototype implementation

In this chapter, the final prototype of the piezoelectric energy harvesting system is presented by integrating all components characterized and developed in previous chapters. The primary goal of the prototype is to validate the experimental findings and demonstrate a functional system capable of powering a low-power IoT sensor using ambient mechanical vibrations.

Based on measurements and performance evaluation, the PPA-2011 transducer is selected as the preferred piezoelectric element due to its power output across the target frequency range (approximately 60 Hz). The goal is to validate this recommendation by connecting the PET to the power conditioning circuit.

To fully implement the prototype, the PPA-2011 is connected to the power conditioning circuit. The PEH is first driven by an ideal sinusoidal signal of 58 Hz. After that, multiple noise signals are tested to see how the system behaves. In the following Table 6.1 the charge times of a 700 μF capacitor are compared under various conditions.

Table 6.1: Charge time of a 700 μF capacitor under various noise conditions

Noise (%)	**Charge Time (s)**
0	15
20	17
60	23
80	28

The capacitor was then able to maintain a constant voltage of 3.3V for 300 ms. In this time, the IoT sensor was able to sense and transmit data multiple times. This shows that the prototype is implemented accordingly and that the system is working. The PET delivers enough power to contribute to a fully functioning piezoelectric harvesting system that can power low-power IoT sensors.

7

Discussion

This chapter evaluates and interprets the findings from the measurements and simulations conducted on the PETs. The performance of each PET model is assessed with respect to its electrical and mechanical characteristics, as well as its robustness under realistic vibration conditions.

7.1. Effect of tip mass on resonance frequency and power output

One of the primary observations is the significant influence of tip mass on the resonance frequency of each PET model. As seen in Tables 5.2 to 5.4, increasing the tip mass consistently lowered the resonance frequency. This behavior is consistent with earlier findings in Chapter 5, where the addition of mass to the free end of a cantilever beam increases the inertia of the system without increasing the stiffness, thus reducing the natural frequency. It was also observed that the resonance peaks of the simulations did not exactly match the measured values. Tables 4.1 and 5.3 have slightly different results.

Furthermore, the increase in the tip mass generally led to a higher peak voltage output. This can be attributed to the greater mechanical deformation of the cantilever, which increases strain-induced charge generation. It was also observed that increasing the tip mass increased the measured optimal load resistance. This can be explained by the fact that as the tip mass increases, the resonance frequency decreases, leading to a longer effective charging period of the internal capacitance of the PET. To match this lower-frequency behavior, a higher load resistance becomes optimal for power transfer.

7.2. Performance across PET models

Each PET has its own unique characteristics:

- **PPA-1021**: Showed a reasonable power output at low tip masses, but there were limitations in pushing the resonance frequency close to 60 Hz. An advantage of this PET is the high internal resistance.
- **PPA-2011**: The most balanced performance was achieved. It gives high power output at resonance near 58 Hz when a tip mass of 1.6 grams was used.
- **PPA-4011**: The model was able to give resonance close to 60 Hz but with a lower peak to peak voltage than the other models possibly due to higher mechanical stiffness. A disadvantage is the low internal resistance that results in less efficient power transfer to the power conditioning circuit.

Among the three, the PPA-2011 proved most suitable for energy harvesting in low-frequency environments, especially for applications targeting the 60 Hz range.

7.3. Impact of noise on energy harvesting

When exposed to band-limited white noise, the performance of all models decreased significantly. The figures show that noise levels of 60-80% of the sine amplitude halve the power output of the PETs. There was no single transducer that was more resistant to noise than the other models. Despite the noise, the optimal

load resistance remained unchanged. This confirms that the internal impedance is not affected in these conditions.

Some more tests on the performance of the PET under noisy conditions were conducted when the whole power conditioning circuit was connected. Measurements showed how fast the storage capacitor was able to charge. In Table 6.1 it is shown that the charge time of the 700 μF capacitor takes much longer to charge when exposed to noise. For the 80% noise level the charge time is almost doubled. This correlates with the power output shown in Figure 5.12.

8

Conclusion

This project has modeled and experimentally validated three different PET models: PPA-1021, PPA-2011 and PPA-4011, to be used in a piezoelectric energy harvester system to power an IoT sensor circuit. The primary objective was to identify and characterize which of the three models would offer best performance in an aircraft vibrational environment and aligns best with the defined Programme of Requirements (PoR).

Initially, for every model its frequency behavior was analyzed in the range of 10-300 Hz by measuring the voltage output of the PET. These tests were repeated with varying tip-mass configurations to investigate how the resonance peaks could be effectively tuned. Following this, detailed analyses of the internal resistance and power output were performed to assess the ability of each model to generate power. Lastly, performance under noisy vibration conditions, representative of real-world scenarios, was evaluated.

Based on these measurements, the PPA-2011 piezoelectric transducer performed best in the PEH system. It demonstrated the best performance by meeting the criteria as outlined in the program of requirements (PoR). The PPA-2011 achieved a power output of 1.14 mW - 1.93 mW depending on the tip-mass adjustment. At approximately 60 Hz, the central target of the PoR's resonance frequency specification, the output reached 1.61 mW. This was considerably more than the PPA-1021 and PPA-4011. Although higher internal resistance generally enhances the efficiency of charging storage capacitors, and the PPA-1021 exhibited slightly higher internal resistance, the substantially higher power output of the PPA-2011 outweighed this advantage. Furthermore, the PPA-2011 remained stable under noisy vibration conditions.

However, it should be noted that several limitations affected the accuracy and completeness of the results. First, replicating the real-world vibrations of an aircraft remains a challenge. In this study, the PETs were tested at their tuned resonance frequencies with superimposed band-limited noise. While this setup provided useful insights into each model's robustness and behavior under noisy conditions, it does not fully capture the unpredictability of in-flight mechanical vibrations.

Second, due to limited resources, it was not possible to precisely extract the values such as the coupling of the electromechanical model. Instead, electrical and mechanical behaviors were evaluated separately.

Lastly, the differences between the datasheet measurements and the measurements of this study are likely influenced by differences in the clamping configuration. The manufacturer's specifications are based on a professional clamp kit. However, the setup shown in Figure 5.1 did not reproduce this configuration, possibly leading to deviations in resonance frequency and mechanical response.

Despite these limitations, the simulations and measurements conducted provided high-quality and accurate performance data with a successful integration of the system as a result.

In conclusion, based on the performance evaluations conducted, the PPA-2011 transducer is clearly aligned best with the defined Programme of Requirements. That is why it is the most suitable piezoelectric model for effectively powering the IoT sensor systems in an aircraft environment.

9

Future work

The results of the power output and behavior of the PEH seemed promising. Enough power can be generated to power a low-power IoT sensor system in a laboratory setting. However, to really integrate a PEH into a complete package and realize its use in an aircraft wing, several tasks can still be done to improve performance and measurements:

9.1. Real-world vibration testing

The research in the current project used simulated vibrations based on frequency assumptions. Future work should use real-world aircraft vibration data to replicate the same vibrations in a laboratory setting. Including noise from other parts of the plane. These tests should also assess how different aircraft models affect the performance of the PEH and whether different configurations are needed. Collaboration with aircraft manufacturers would allow access to such data and may also include real-world testing on aircraft.

9.2. Extract complete electromechanical modeling.

Future research should accurately measure the acceleration and displacement of PZT to extract the coupling coefficients of the transducer models. This would enable for more precise simulations in different situations and environments.

9.3. Create a physics model.

By creating a physics model in the future, long-term stability of PZT materials exposed to different temperatures, resonance frequencies, and mechanical fatigue can be simulated. These models can be created through finite element simulations. For example, using COMSOL. This option was explored during this project; however, due to time constraints, the results from this model could not be analyzed. One of the constraints was that there was no complete electromechanical model. This limited the simulation possibilities. However, with future work, this simulation can be implemented.

9.4. Thermal performance

In the future, temperature-controlled experiments should be conducted to assess the performance of the PEH system under different temperature ranges. The ceramic used in the PEH harvester, PZT-5H, is influenced by temperature [8]. Since temperatures on aircrafts can range between -40 and +85 degrees Celsius it is important to assess material behavior and power performance.

9.5. Regulatory and environmental testing

Validate the system against relevant aerospace standards such as EUROCAE ED-14G. This will ensure that the PEH is in compliance with international regulation and that it is able to implement the system for commercial use.

9.6. Self-tuning harvester systems

One of the main drawbacks of the PEH harvester is that its performance is mainly centered around the resonance frequency. Research has been done on ways to improve the performance of a PEH to a broader frequency range. In the future, structural and control-based techniques can be explored to widen the bandwidth of the PEH. These options include:

1. Incorporating self-movable mass into the cantilever beam. This mass will arrange itself on the beam so that the complete PEH resonates at the current surrounding vibration frequency. The implementation of this is discussed in [12]. During the project, this implementation was tested using 3D printed parts. Although the mass did move by itself and was able to position itself on the basis of the frequency, more testing has to be done to produce viable measuring data. In addition, the parts were fragile and the results could be improved by using specialized machines to create the accurate parts with the constraints needed to implement this system effectively.

2. Tuning of the cantilever beam with an adaptive clamping system as described in [14]. Here custom-made clamps can automatically alternate depending on the surrounding vibration frequency.

Bibliography

[1] Akhil Basutkar, Kunal Baruah, and Shashidhar K. Kudari. "Frequency Analysis of Aircraft Wing Using FEM". In: *Proceedings of the International Conference on Intelligent Manufacturing and Energy (ICIME)*. Chapter in conference proceedings. Hyderabad, India: Springer, 2020. DOI: 10.1007/978-981-15-1124-0_46. URL: https://www.researchgate.net/publication/338539277.

[2] Jordi Brufau-Penella et al. *ELECTROMECHANICAL MODEL OF a MULTI-LAYER PIEZOELECTRIC CANTILEVER*. Tech. rep. 2006.

[3] Midé Technology Corporation. *PPA PRODUCTS Datasheet User Manual*. Mar. 2016. URL: https://www.mouser.com/datasheet/2/606/ppa-piezo-product-datasheet-844547.pdf?srsltid=AfmBOoo-szTBjH8tyatQSuoWfsOo3DVeMi5GwFvAAEmFC6HJl1IhF9pT.

[4] Pierre Curie et al. *A History of Piezoelectricity*. URL: https://mastersonics.com/documents/mmm_basics/general_info/ultrasonics_faq/ultrasonics_physics.pdf.

[5] Sijun Du. *Energy-efficient Interfaces for Vibration Energy Harvesting*. Jan. 2018. DOI: 10.17863/cam.17227. URL: https://www.repository.cam.ac.uk/items/1f97bc2e-0397-47a6-b4dc-992c366e7939.

[6] fujicera@kabosu. *PZT Material Selection Guide* -. Nov. 2024. URL: https://www.fujicera.co.jp/en/feature/4164/.

[7] Moncef Hammadi, Jean-Yves Choley, and Faïda Mhenni. "A multi-agent methodology for multi-level modeling of mechatronic systems". In: *Advanced Engineering Informatics* 28 (Aug. 2014). DOI: 10.1016/j.aei.2014.03.005.

[8] Matthew W. Hooker. *Properties of PZT-Based Piezoelectric Ceramics Between -150 and 250 C*. Sept. 1998. URL: https://ntrs.nasa.gov/citations/19980236888.

[9] Hottinger Brüel & Kjær. *LDS Permanent Magnet Vibration Systems: V100, V200, V400, and V450 Series*. System Data Sheet BU 3105-14. HBK - Hottinger Brüel & Kjær. Jan. 2023. URL: https://www.bksv.com/en/instruments/vibration-testing-equipment.

[10] Don Isarakorn et al. "Epitaxial piezoelectric MEMS on silicon". In: *Journal of Micromechanics and Microengineering* 20 (Apr. 2010). DOI: 10.1088/0960-1317/20/5/055008.

[11] T.M. Kamel. "Poling and switching of PZT ceramics : field and grain size effects". English. Phd Thesis 1 (Research TU/e / Graduation TU/e). Chemical Engineering and Chemistry, 2007. ISBN: 978-90-386-1088-7. DOI: 10.6100/IR628929.

[12] Sallam A. Kouritem et al. "Automatic Resonance Tuning Technique for an Ultra-Broadband Piezoelectric Energy Harvester". In: *Energies* 15.19 (2022). ISSN: 1996-1073. DOI: 10.3390/en15197271. URL: https://www.mdpi.com/1996-1073/15/19/7271.

[13] Martin Kucera et al. "Design-dependent performance of self-actuated and self-sensing piezoelectric-AlN cantilevers in liquid media oscillating in the fundamental in-plane bending mode". In: *Sensors and Actuators B Chemical* 200 (Apr. 2014), pp. 235–244. DOI: 10.1016/j.snb.2014.04.048. URL: https://doi.org/10.1016/j.snb.2014.04.048.

[14] Dong-Gyu Lee et al. "Autonomous Resonance-Tuning Mechanism for Environmental Adaptive Energy Harvesting". In: *Advanced Science* 10.3 (Nov. 2022). DOI: 10.1002/advs.202205179. URL: https://doi.org/10.1002/advs.202205179.

[15] Jing-Feng Li. *Fundamentals of Piezoelectricity*. First Edition. WILEY-VCH GmbH, 2021.

[16] Christopher Shawn McGahey. *HARNESSING NATURE'S TIMEKEEPER: A HISTORY OF THE PIEZOELECTRIC QUARTZ CRYSTAL TECHNOLOGICAL COMMUNITY (18801959)*. May 2009.

[17] *Piezoelectricity Basics*. URL: https://www.ctscorp.com/Resources/Blog/Piezo-Basics.

[18] Aldo Romani et al. “Joint Modeling of Piezoelectric Transducers and Power Conversion Circuits for Energy Harvesting Applications”. In: *IEEE Sensors Journal* 13.3 (Sept. 2012), pp. 916–925. DOI: 10.1109/jsen.2012.2219580. URL: https://doi.org/10.1109/jsen.2012.2219580.

[19] S Roundy and P K Wright. “A piezoelectric vibration based generator for wireless electronics”. In: *Smart Materials and Structures* 13.5 (Aug. 2004), pp. 1131–1142. DOI: 10.1088/0964-1726/13/5/018. URL: https://doi.org/10.1088/0964-1726/13/5/018.

[20] Nurettin Sezer and Muammer Koç. “A comprehensive review on the state-of-the-art of piezoelectric energy harvesting”. In: *Nano Energy* 80 (2021), p. 105567. ISSN: 2211-2855. DOI: https://doi.org/10.1016/j.nanoen.2020.105567. URL: https://www.sciencedirect.com/science/article/pii/S2211285520311411.

[21] Rebecca Thompson, Thalia Hull, and Dr. Michael Rice. *ELIMINATING WIRING IN AIRCRAFT INSTRUMENTATION THROUGH ENERGY HARVESTING*. Nov. 2018. URL: https://repository.arizona.edu/handle/10150/631669.

[22] K. Uchino. “1 - The development of piezoelectric materials and the new perspective”. In: *Advanced Piezoelectric Materials*. Ed. by Kenji Uchino. Woodhead Publishing Series in Electronic and Optical Materials. Woodhead Publishing, 2010, pp. 1–85. ISBN: 978-1-84569-534-7. DOI: https://doi.org/10.1533/9781845699758.1. URL: https://www.sciencedirect.com/science/article/pii/B9781845695347500017.

[23] Yu Xiao, Qinkai Han, and Nan Wu. “Piezoelectric energy harvesting: a review of energy sources, structures, and working mechanisms in high-frequency excitations and operations”. In: *Smart Materials and Structures* (Jan. 2025). DOI: 10.1088/1361-665x/adadcc. URL: https://doi.org/10.1088/1361-665x/adadcc.

Appendices

A

Appendix

A.1. Frequency Response Simulations

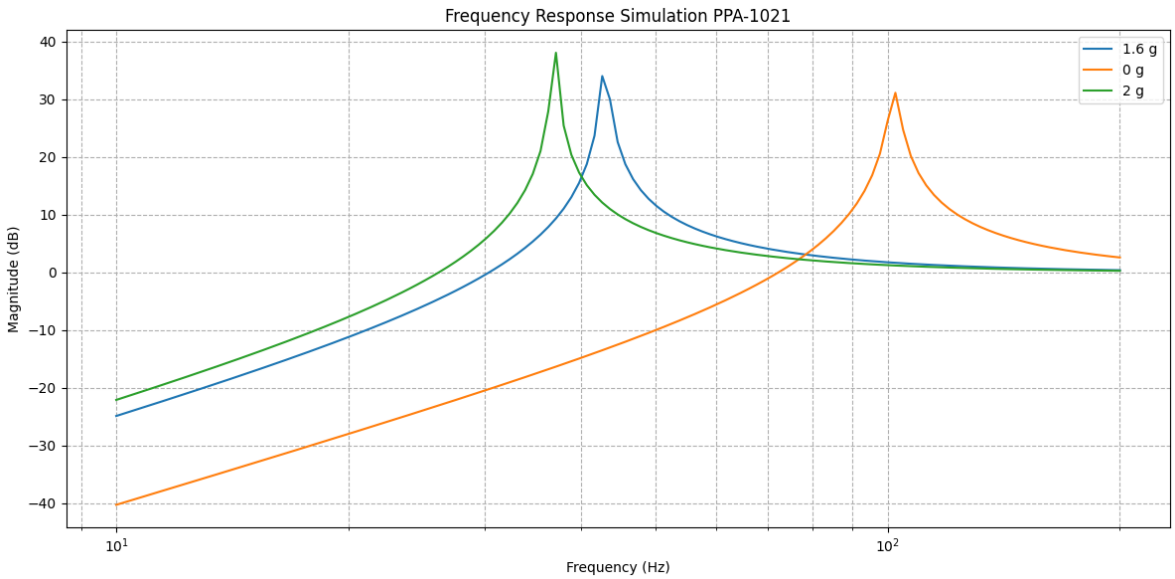

Figure A.1: Frequency Response PPA-1021 simulation

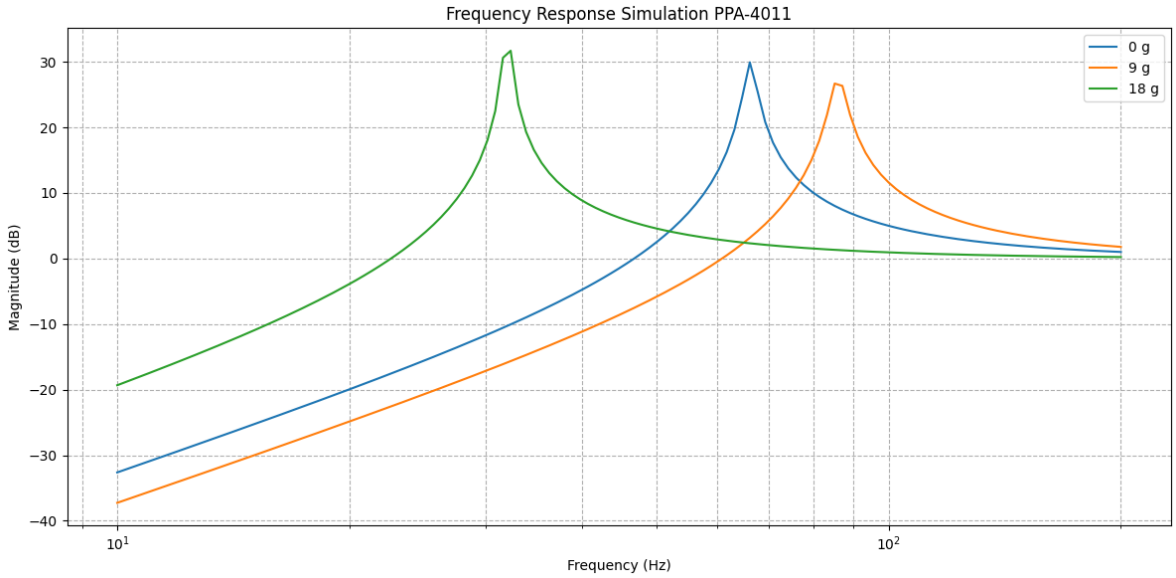

Figure A.2: Frequency Response PPA-4011 simulation

A.2. Python code for noisy conditions

```python
import numpy as np
import matplotlib.pyplot as plt

Fs = 16000           # Sampling rate (16 000 samples/sec)
duration = 1.0       # Duration = 1 second
N = int(Fs * duration)  # Total samples = 16 000
t = np.linspace(0, duration, N, endpoint=False)

#Sine wave
sine_wave = np.sin(2 * np.pi * 58 * t)

#Generate white noise and band-pass filter between 10  300   Hz via FFT
noise = np.random.randn(N)
noise_fft = np.fft.rfft(noise)
freqs = np.fft.rfftfreq(N, 1 / Fs)

band_mask = (freqs >= 10) & (freqs <= 300)
filtered_noise_fft = noise_fft * band_mask
filtered_noise = np.fft.irfft(filtered_noise_fft, n=N)

#Scale noise to 0.2 of noise amplitude
noise_amplitude = 0.6
filtered_noise = filtered_noise / np.max(np.abs(filtered_noise)) * noise_amplitude

#sine + noise
composite_wave = sine_wave + filtered_noise

#normalzie to +-1
composite_wave /= np.max(np.abs(composite_wave))

#Save to CSV
filename = "58_0_6_amp.csv"
np.savetxt(filename, composite_wave, delimiter=",")

plt.figure(figsize=(8, 3))
plt.plot(t[:int(Fs)], composite_wave[:int(Fs)])
plt.title("58 Hz Sine + 10  300   Hz Noise")
plt.xlabel("Time (s)")
plt.ylabel("Amplitude (normalized)")
plt.grid(True)
plt.tight_layout()
```

```
42 plt.show()
43
44 print(f"Waveform saved as '{filename}' with {N} samples at {Fs} Hz sampling rate.")
```

Listing A.1: Python code sine wave + noise